Efficient RFI suppression in SAR using a LMS adaptive filter with sidelobe suppression integrated with the range-Doppler algorithm

Richard T. Lord and Michael R. Inggs
Radar Remote Sensing Group, Dept. EE, University of Cape Town
Private Bag, Rondebosch 7701, South Africa
Tel: +27 21 650 3756 Fax: +27 21 650 3465
Email: rlord@rrsg.ee.uct.ac.za Web: http://rrsg.ee.uct.ac.za

Abstract — The LMS adaptive filter has been used successfully to suppress radio frequency interference (RFI) from SAR images. This paper describes a method to efficiently implement this filter by integrating it with the range-Doppler algorithm. A technique to reduce the sidelobes created by the filter is described and illustrated on simulated data and on real P-Band data.

INTRODUCTION

Radio frequency interference (RFI) is often a major problem for low frequency synthetic aperture radar (SAR) systems, operating in the VHF/UHF Band. A number of interference suppression algorithms have been described in the literature [1, 2, 3, 4, 5, 6, 7, 8], many of which require a great deal of computation. This paper describes how computational savings may be achieved by integrating the LMS adaptive filter with the range-Doppler algorithm. Furthermore, a technique is described to reduce range sidelobes, which arise as an unwanted by-product of the RFI suppression stage. This technique is demonstrated on simulated data and on real P-Band data.

EQUIVALENT TRANSFER FUNCTION

The integration of the LMS adaptive filter and the range-Doppler algorithm is achieved by multiplying the equivalent transfer function of the interference suppression stage with the transfer function of the range compression stage, thereby creating a new transfer function which implements interference suppression and range compression simultaneously. Assuming that this combined transfer function is valid over many range lines (which has been confirmed by the authors on P-Band and VHF-Band data), significant computational savings can be realised. The technical details of this method have been submitted for journal review, and are therefore only summarised in this paper.

Once the tap weights of the LMS adaptive filter have converged, the filter may be represented in block-diagram form as shown in Fig. 1. The equivalent transfer function $H(\omega)$ of this filter is given by

$$H(\omega) = \frac{E(\omega)}{D(\omega)} = 1 - F(\omega)\,G(\omega) \tag{1}$$

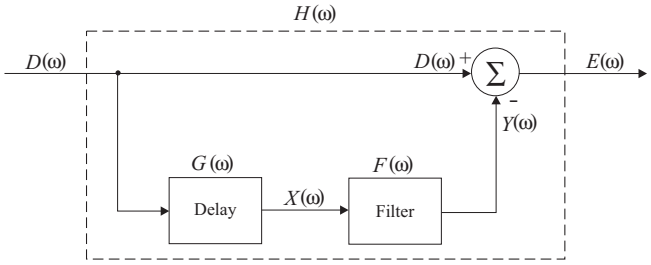

Figure 1. Block diagram of LMS adaptive filter with tap weights kept constant

where $G(\omega)$ is the transfer function of the time-delay Δ, given by

$$G(\omega) = e^{-j\omega\Delta} \tag{2}$$

and $F(\omega)$ is the Fourier Transform of the *time-reversed* weight vector $\mathbf{W}$. Range compression in the frequency domain is accomplished by multiplying the received signal with a matched filter $M(\omega)$, which is typically the complex conjugate of the transmitted pulse spectrum. The combined transfer function $T(\omega)$ is therefore given by

$$T(\omega) = H(\omega)\,M(\omega) \tag{3}$$

This transfer function will simultaneously suppress RFI and perform range compression on the raw SAR image.

SIDELOBE REDUCTION

Any interference suppressing filter will corrupt the desired signal with sidelobes. Abend and McCorkle [1] have described a sidelobe reducing procedure which has some similarities to the sidelobe reduction procedure presented in this paper. Fig. 2 shows a graphical illustration of the technique. In Fig. 2 (a) the RFI contaminated signal passes through the LMS adaptive filter $H(\omega)$, yielding a signal free from RFI, but with introduced sidelobes. It is assumed that the RFI suppression is done perfectly, i.e. that there is no RFI present in the filtered output. In Fig. 2 (b), the output from (a) is subtracted from the unfiltered signal, the result of which is passed again through

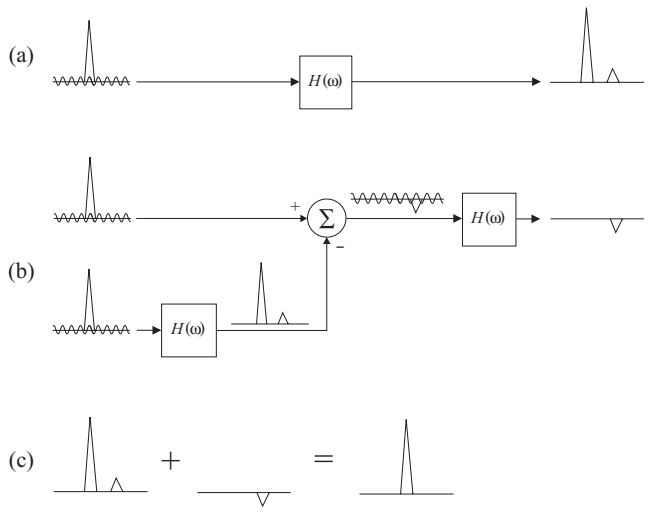

Figure 2. Graphical illustration of sidelobe reduction procedure. The large triangle symbolises the wanted compressed target, the small triangle the unwanted sidelobe and the sinusoidal waveform the unwanted RFI interference.

the LMS adaptive filter, yielding a cleaned signal which contains only the (negative) sidelobe. It is assumed that the sidelobe embedded in the RFI is already so small, that the output of the LMS adaptive filter does not contain any sidelobes of the sidelobe. Adding the results of (a) and (b) together yields the result shown in Fig. 2 (c), which is just the cleaned signal without any sidelobes.

The complete sidelobe reduction procedure is shown in block diagram form in Fig. 3. It can be shown that the overall transfer function is

$$H'(\omega) = \frac{E'(\omega)}{D(\omega)} = H(\omega)\left[2 - H(\omega)\right] \tag{4}$$

The above assumption, that the "sidelobes of the sidelobe" are negligible, is not always valid. The same procedure that was described above to suppress the original sidelobe can be used to suppress the "sidelobe of the sidelobe". The overall transfer function of this so-called "second-order"

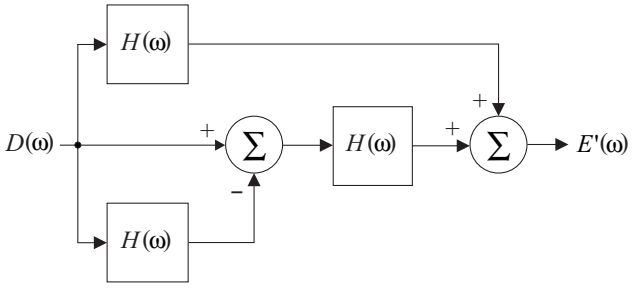

Figure 3. Block diagram of sidelobe reduction procedure, where $H(\omega)$ is the transfer function of the LMS adaptive filter.

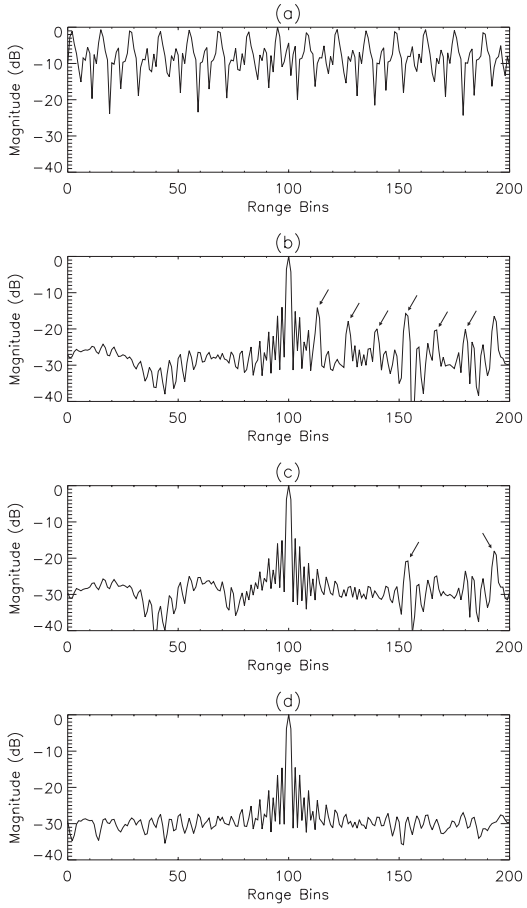

Figure 4. Simulation result of sidelobe reduction procedure. (a) RFI contaminated echo return. (b) Filtered echo return with no sidelobe reduction. Arrows point at unwanted sidelobes. (c) Filtered echo return with first-order sidelobe reduction. (d) Filtered echo return with second-order sidelobe reduction.

sidelobe reduction procedure can be shown to be

$$H'_{2nd}(\omega) = H(\omega)\left[3 - 3H(\omega) + H(\omega)^2\right] \tag{5}$$

and the overall transfer function of the "third-order" sidelobe reduction procedure can be shown to be

$$H'_{3rd}(\omega) = H(\omega)\left[4 - 6H(\omega) + 4H(\omega)^2 - H(\omega)^3\right] \tag{6}$$

The matched filter $M(\omega)$ in (3) will now be multiplied with $H'(\omega)$ instead of $H(\omega)$, thus incorporating the sidelobe reduction procedure, leading to a very efficient implementation.

SIMULATION RESULTS

Fig. 4 summarises simulation results which verify the effectiveness of the sidelobe reduction procedure. In Fig. 4 (a) the range compressed, RFI contaminated signal is shown. The target is swamped by RFI and cannot

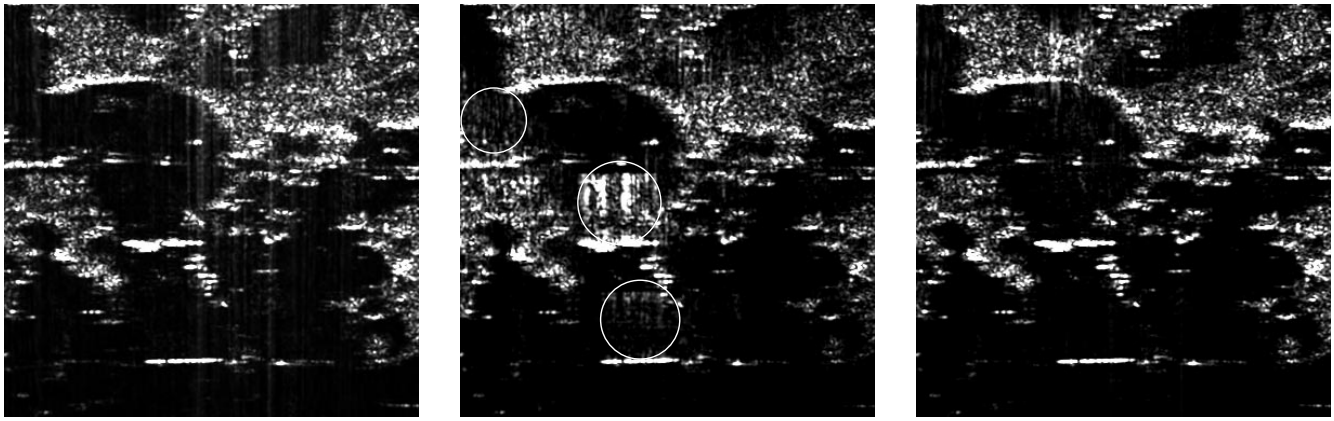

Figure 5. Real results obtained from P-Band data supplied by the DLR, Oberpfaffenhofen, Germany. (a) RFI contaminated image. (b) Filtered image without any sidelobe reduction. The circles indicate regions with very high sidelobes. (c) Filtered image with third-order sidelobe reduction.

be detected. Fig. 4 (b) shows the result obtained after cleaning the signal, with no sidelobe reduction applied. The arrows in the figure point to clearly visible sidelobes. Fig. 4 (c) and (d) show the cleaned signal with first-order and second-order sidelobe reduction applied respectively. There is clearly a remarkable reduction in sidelobe levels visible.

P-BAND DATA RESULTS

Fig. 5 (a) displays a zoomed-in portion of a RFI contaminated P-Band image supplied by the DLR, Oberpfaffenhofen. This region contained especially bright targets, which resulted in unacceptably high sidelobes depicted in Fig. 5 (b). After cleaning this image with a third-order sidelobe reduction procedure, the image shown in Fig. 5 (c) was obtained, which is clearly a vast improvement. However some of the original interference started appearing again. Thus the original RFI suppression capability of the filter is compromised by applying the sidelobe reduction procedure.

CONCLUSIONS

This paper has described how the equivalent transfer function of the LMS adaptive filter may be obtained and combined with the matched filter transfer function of the range compression stage of the range-Doppler SAR processing algorithm. This paper has described a sidelobe reduction procedure, whose equivalent transfer function can be written in terms of the transfer function of the LMS adaptive filter. Thus a combined transfer function can be obtained which implements RFI suppression, sidelobe reduction and range compression simultaneously, leading to a very efficient implementation.

ACKNOWLEDGMENTS

The authors would like to thank Stefan Buckreuss from the DLR for supplying the raw P-Band E-SAR data.

REFERENCES

[1] K. Abend and J. McCorkle, "Radio and TV interference extraction for ultra-wideband radar," in *Algorithms for Synthetic Aperture Radar Imagery II* (D.A. Giglio, ed.), SPIE, Orlando, FL, vol. 2487, pp. 119–129, April 1995.

[2] M. Braunstein, J. Ralston and D. Sparrow, "Signal processing approaches to radio frequency interference (RFI) suppression," in *Algorithms for Synthetic Aperture Radar Imagery* (D.A. Giglio, ed.), SPIE, Orlando, FL, vol. 2230, pp. 190–208, April 1994.

[3] S. Buckreuss, "Filtering Interferences from P-Band SAR Data," *Proc. European Conference on Synthetic Aperture Radar, EUSAR'98*, Friedrichshafen, Germany, pp. 279–282, May 1998.

[4] T. Koutsoudis and L. Lovas, "RF Interference Suppression in Ultra Wideband Radar Receivers," in *Algorithms for Synthetic Aperture Radar Imagery II* (D.A. Giglio, ed.), SPIE, Orlando, FL, vol. 2487, pp. 107–118, April 1995.

[5] C.T.C. Le, S. Hensley and E. Chapin, "Removal of RFI in Wideband Radars," *Proc. IEEE Geoscience Remote Sensing Symp., IGARSS'98*, Seattle, Washington, vol. 4, pp. 2032–2034, July 1998.

[6] R.T. Lord and M.R. Inggs, "Approaches to RF Interference Suppression for VHF/UHF Synthetic Aperture Radar," *Proc. IEEE South African Symp. on Communications and Signal Processing*, COMSIG'98, Cape Town, South Africa, pp. 95–100, September 1998.

[7] T. Miller, J. McCorkle and L. Potter, "Near-least-squares radio frequency interference suppression," in *Algorithms for Synthetic Aperture Radar Imagery II* (D.A. Giglio, ed.), SPIE, Orlando, FL, vol. 2487, pp. 72–83, April 1995.

[8] B. Widrow, J.R. Glover, Jr., J.M. McCool, J. Kaunitz, C.S. Williams, R.H. Hearn, J.R. Zeidler, E. Dong, Jr., and R.C. Goodlin, "Adaptive Noise Cancelling: Principles and Applications," *Proc. IEEE*, vol. 63, no. 12, pp. 1692–1716, December 1975.